strain
An International Journal for Experimental Mechanics

The *b*-Value Analysis for the Stability Investigation of the Ancient Athena Temple in Syracuse

A. Carpinteri, G. Lacidogna and A. Manuello

Department of Structural Engineering & Geotechnics, Politecnico di Torino, Corso Duca degli Abruzzi 24 – 10129 Torino, Italy

ABSTRACT: Some of the most significant architectural works are monumental masonry constructions. Among these, the Cathedral of Syracuse can be viewed as a fundamental element in the cultural heritage of Europe. For the preservation of these monuments, it is necessary to assess their durability by taking into account cumulative damage and cracking conditions in the structures. The paper describes the methods used by the authors to determine the conditions of the materials and the crack patterns in the stonework structures of the Cathedral. In particular, the acoustic emission (AE) technique is used to evaluate the time dependence of damage and the onset of critical conditions in a pillar, which is part of the vertical load-bearing structures. The authors show that the damage evolution in the stonework structures, experimentally investigated *in situ* by the AE technique, can be described by a power law characterised by a non-integer exponent, β_t. In this way, the time dependence of damage is evaluated by working out the β_t exponent and making a prediction of the stability conditions of the structure. Furthermore, the achievement of the critical condition is characterised through another synthetic parameter, the *b*-value of the Gutenberg-Richter law. The *b*-value systematically changes during the different stages of the failure process and tends to 1.0 as the structure reaches the final collapse. In the present study, this behaviour is documented by several AE tests carried out on specimens of different dimensions extracted from the pillar. In addition, these results are compared with the AE data obtained from the *in situ*-monitored pillar.

KEY WORDS: *acoustic emission, b-value analysis, cultural heritage, experimental evaluation, monumental masonry*

Introduction

The Cathedral of Syracuse can be viewed as a fundamental element in the history and cultural heritage of Europe. In the last few years, this monument has been intensively studied in order to evaluate the structural state of preservation. The Cathedral of Syracuse was built in different phases over the ancient Greek 'Temple of Athena' of the 5th century BC and modified along the centuries. The pillars of the central nave, obtained by cutting the walls of the temple cell, show a complex situation of damage and repairs [1].

A programme of investigation was recently developed with the objective of studying the vulnerability of the building to seismic events through analytical models as well as of designing provisional measures of safety to be taken. The structure analysed has been affected over the centuries by violent earthquakes that have wasted the entire area of Syracuse and the neighbouring regions. Some of these seismic events contributed towards making the stability of the monument particularly critical. Today the structural condition of the Cathedral is precarious because of the many construction events that marked the history of the Athena's temple during the last century. In the last few years, several restoration and preventive works have been undertaken by the Syracuse Superintendence for Cultural Heritage to avoid the collapse of the building in the event of an earthquake.

Of late, the authors have been working on the development of a method for the assessment of materials and structures based on the spontaneous release of pressure waves during the evolution of damage. This monitoring technique, referred to as 'acoustic emission' (AE), is non-invasive and non-destructive and is therefore ideal for the control of historic and monumental structures in seismic areas [2–4]. Once the damaged portion of a structure has been located, it becomes possible to evaluate the stability of the evolving damage, which may either come gradually to a halt or propagate at an ever faster rate. In this study, the AE technique was used to

doi: 10.1111/j.1475-1305.2008.00602.x

determine the level of damage in a pillar that was part of the vertical bearing structure of the Cathedral of Syracuse (Sicily). Remembering the partial collapse of the Noto Cathedral and its causes [5], the Superintendent M. Muti of the Syracuse Cultural Heritage Office supported an experimental and analytical research into the state of the Cathedral.

Description of the Syracuse Cathedral

In the 6th century AD, the 5th century BC Greek temple of Athena in Syracuse, was transformed into a Catholic Church, and thence became the Cathedral of the City; the building was frequently modified along the centuries until the present configuration (see Fig. 1) [1, 6].

The pillars of the Cathedral are peculiar in that they had been cut out of the stonework walls of the internal cell of the Greek temple. The pillars show not only several repaired areas and replacements, but also several cracks. In order to evaluate their state of preservation, the extension and depth of the replacements and the presence of internal defects, an investigation programme was planned by the Superintendence and the Politecnico di Milano. As a first step, a survey of the pillars with an accurate mapping of the superficial materials, the defects, cracks and the morphology was carried out. The crack pattern was classified, accurately documented and reported on the geometrical survey. The cracks frequently display a vertical pattern because of compressive stresses, the action of which is often combined with the compressive bending stresses caused by frequent earthquakes. In some cases, the corners and parts of the stone blocks were expelled. The mortar fillings in these cases are trials to locally repair the damages. In the survey, the repaired cracks were cleared in order to evaluate the damage evolution.

On the basis of this detailed survey, non-destructive techniques (NDT) tests were performed in order to investigate the depth of the damage. The complementarity of the NDTs already studied in Refs [7–9], could be successfully exploited to diagnose the extent of damage to the pillars. Furthermore, a monitoring of the development of the cracks for *c.* 2 years showed an evident trend towards an increase in the size of cracks in some of the pillars (nos 18, 19, 29 and 30), which suggested a further check of the damage by AE technique (Fig. 2).

The Monitored Structure

The AE monitoring procedure was performed on a pillar of the Cathedral of Syracuse. The temple had 14 columns along the sides and six at the front, and some of them, belonging to the peristyle and the stylobate, can still be identified. In the layout of the Cathedral shown in Fig. 2A, all the pillars and the columns inside the building are marked with a progressive number.

Basically, the Doric columns are marked with numbers in three ranges (1–8; 22, 23; 33–40) and the pillars carved from the calcareous stone masonry of the temple cell are identified with the remaining numbers. As mentioned above, from the survey of the cracks, it was determined that the pillars in the most critical conditions were nos 18, 19, 29 and 30, all of them located near the end of the central nave (circle in Fig. 2A). These pillars show an appreciable degree of deterioration, because of the presence of added layers of plaster and conspicuous cracks, which in some cases seem to cut the constituent stone blocks. Pillar 19, selected for the application of the AE monitoring technique, is shown in the axonometric view in Fig. 2C. The pillar, save for a few strengthening works performed according to the Syracuse

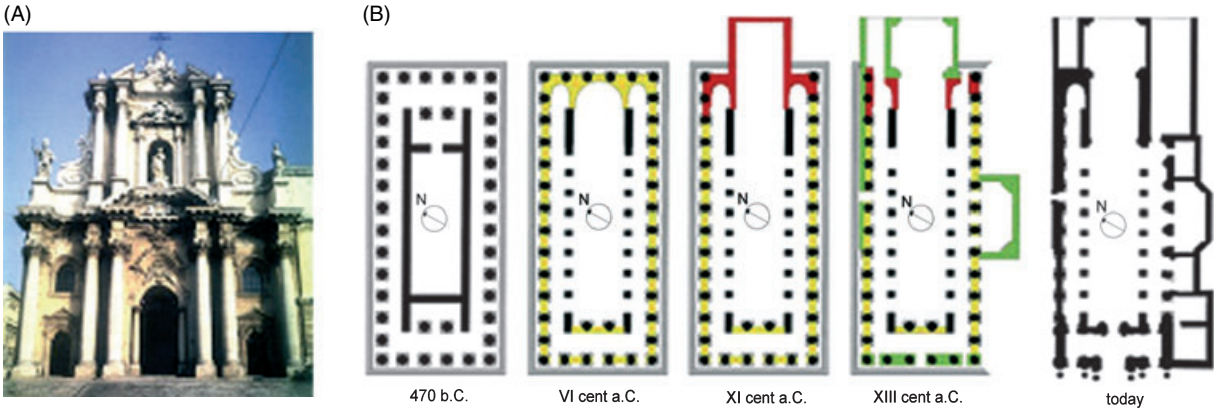

Figure 1: The Syracuse Cathedral (A) and its evolution (B)

doi: 10.1111/j.1475-1305.2008.00602.x

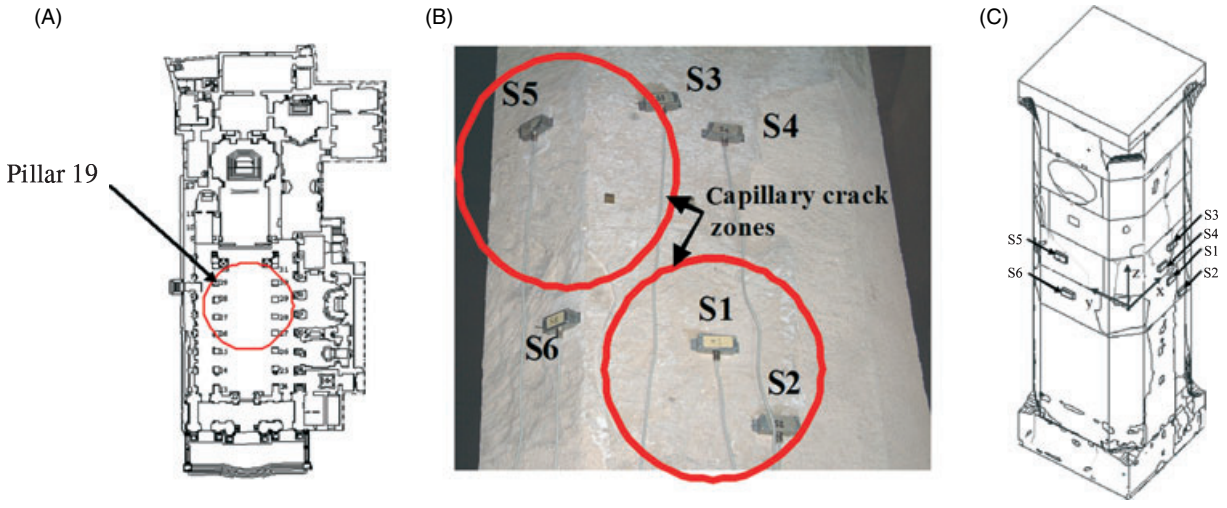

Figure 2: Plan of the Syracuse Cathedral. Pillars 19, 20, 30 and 31 are pointed out (A) AE sensors arrangement on pillar 19: view (B), and axonometric scheme (C)

Superintendence for Cultural Heritage during a restoration process in 1926, was thought to be made of limestone blocks installed during the initial construction of the temple dedicated to Athena in the 5th century BC. Several investigations revealed the presence of brick masonry parts ascribed to the interventions at the beginning of the 20th century [10, 11]. The reduced stiffness of these parts is the probable cause of the damage developed in the stones. Interesting numerical models of the vertical bearing structures of the Cathedral are presented in literature [10–12]. Particularly, in Carpinteri *et al.* [11, 12], the numerical results are in accordance to the AE monitoring experimental evidence.

Application of the AE Technique

A number of techniques have been developed to detect and study crack growth in brittle rock fracture. The most common of these involves the use of strain gauges to measure slight changes in sample deformation that can be related to the closing and opening of cracks [13, 14]. To a lesser extent, AE monitoring has been used to correlate the number of acoustic events with various strain gauge responses [15–17]. Other techniques have involved the use of photoelastics, optical diffraction patterns, scanning electron microscopes, laser speckle interferometry, ultrasonic probing and electrical resistivity [18]. Many of these NDT work by introducing some type of energy into the system to be analysed. In AE tests, the energy input is the mechanical stresses produced by the structure itself through the application of loads [18].

By monitoring a structure by means of the AE technique, it becomes possible to detect the occurrence and evolution of stress-induced cracks. Cracking, in fact, is accompanied by the emission of elastic waves which propagate within the bulk of the material. These waves can be received and recorded by piezoelectric (PZT) transducers applied to the external surface of the structural elements. The signal is therefore analysed by a measuring system counting the emissions that exceed a certain voltage threshold measured in volts. In isotropic and homogeneous materials, the AE waves propagate through the solid, according to straight rays moving at the same velocity in every direction, until they reach the outer surface, where they are captured by *ad hoc* sensors [2–4, 19]. As for material attenuation properties, it is known that they depend on the frequency range: higher frequency components propagate in materials with greater attenuation. If the material contains inhomogeneities, the wavelength needs to be larger of the maximum inhomogeneity in order for the wave to 'pass through' without significant modifications in its waveform [19, 20].

AE equipment and '*in situ*' applications details

The leading-edge equipment adopted by the authors consists of six units (USAM, Costruzioni Progettazioni Elettroniche D' Angelosante s.a.s., Rome, Italy), that can be synchronised for multi-channel data processing. The most relevant parameters acquired from the signals (frequencies in a range between 50 and 800 kHz, arrival time, amplitude, duration, number of events and oscillations) are stored in the USAM memory and then downloaded onto a PC for a multi-channel data processing. On each side of element 19 an evident cracking pattern is observed. The AE sensors have been applied on the middle part of the pillar as shown in Fig. 2B,C. In Fig. 2B the zones with capillary vertical cracks are indicated by

doi: 10.1111/j.1475-1305.2008.00602.x

circles. The arrangement of AE sensors is represented in Fig. 2B according to the scheme reported in Fig. 2C. The sensors were glued with silicone resin on two faces of the pillar.

Results of the monitoring procedure

The monitoring procedure began at 11:00 AM on 19 September 2006 and ended at 12:20 PM on 21 January 2007. The data collected were analysed in order to interpret the evolution of damage and determine the positions of AE sources within the pillar. The AE signal received by the transducers is processed by an analyser which counts the oscillations exceeding a certain voltage threshold. This makes it possible to plot cumulative curves reflecting the count number as measured continuously throughout the monitoring period. This method, referred to as *Ring-Down Counting*, is widely used for defect detection purposes (see Fig. 3). As a first approximation, in fact, the count number N, i.e. oscillations per unit time (differential function) can be compared with the quantity of energy released during the monitoring process, and the relative sums (cumulative function) may be assumed to increase proportionately with the widening of the damaged zone. Needless to say, this assumption applies only if the damage evolves slowly [21–23]. Figure 3 shows the diagrams of the differential and cumulative functions obtained from the count numbers measured per day on pillar 19. These charts were plotted starting from the date of application of the sensors to the pillar up to the time when they were definitively removed. During the monitoring period, the threshold level for the input signals from the PZT transducers was always set to 100 μV. Based on the authors' experience, this threshold level is the most significant for the reception of AE signals during a damage process in non-metallic materials such as concrete and masonry [3, 4, 23, 24].

From the charts it can be seen that the pillar is actually undergoing a deterioration process. It should be noted that during the monitoring period strong seismic actions were recorded in the area within a radius of *c.* 50 km around the city of Syracuse. If we examine the chart illustrating the differential function of AE counts, we can see sudden increases in the oscillation peaks occurring at certain intervals over time. These sudden increments are matched by leaps in the cumulative functions of AE counts and reveal an interesting correlation between the AE activities determined experimentally and seismic events. The AE counts in other time intervals seem to evolve in a virtually linear manner. It may therefore be assumed that the discontinuities in the cumulative function reflect the critical moments during which the amount of energy released – because of the evolution of damage in the structure – is the highest.

Detection and time dependence of damage

We consider that during the microcrack propagation the dissipated energy, E, in a structural element is proportional to the cumulative number of AE counts, N [3, 4, 23, 24]. In this way, the time dependence of the structural damage observed during the monitoring period, identified by the parameter η, can also be correlated with the rate of propagation of the

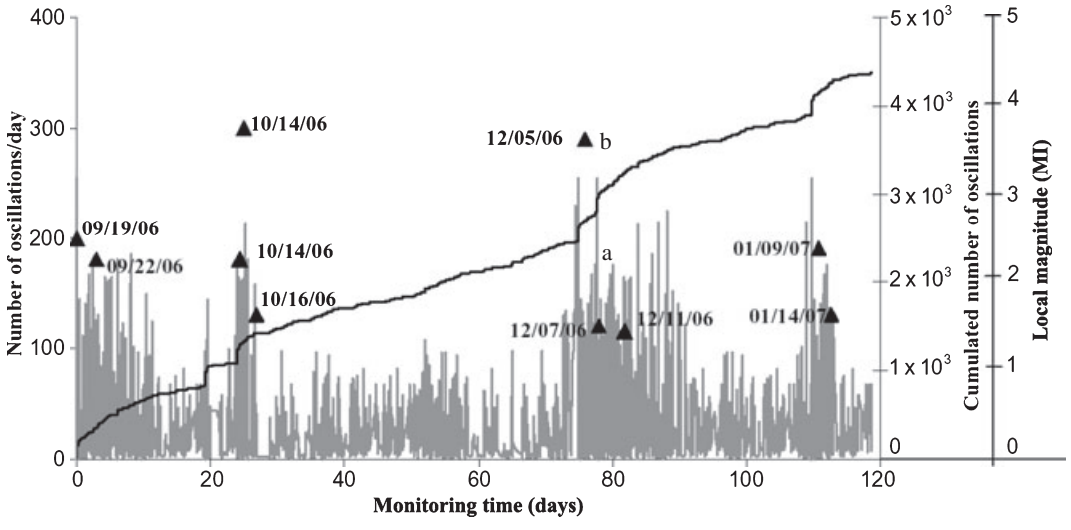

Figure 3: Differential (a) and cumulated (b) number of AE oscillations during the monitoring time on the pillar 19. The most relevant seismic events, with the local magnitude value, occurred during the same period are also indicated in the graph. Earthquake data for the period were obtained from the website http://www.ct.ingv.it/Sismologia/GridSism.asp published by the Seismic Data Analysis Group of Catania (Gruppo di Analisi Dati Sismici, INGV-CT)

doi: 10.1111/j.1475-1305.2008.00602.x

microcracks. If we express the ratio between the cumulative number of AE counts recorded during the monitoring process, N, and the number obtained at the end of the observation period, N_d, as a function of time, t, we get the damage versus time dependence on AE:

$$\eta = \frac{E}{E_d} = \frac{N}{N_d} = \left(\frac{t}{t_d}\right)^{\beta_t} \quad (1)$$

In Equation (1), the values of E_d and N_d do not necessarily correspond to critical conditions ($E_d \leq E_{\max}$; $N_d \leq N_{\max}$) and the t_d parameter must be considered as the time during which the structure has been monitored. By working out the β_t exponent from the data obtained during the observation period, we can make a prediction as to the structure's stability conditions. If $\beta_t < 1$, the damaging process slows down and the structure evolves towards stability conditions, in as much as energy dissipation tends to decrease; if $\beta_t > 1$ the process diverges and becomes unstable; if $\beta_t \cong 1$ the process is metastable, i.e. though it evolves linearly over time, it can reach either stability or instability conditions indifferently [3, 4]. During the observation period, which lasted 121 days, the number of AE counts was ≅4300 (Fig. 3). The data obtained with the AE technique yielded a slant $\beta_t \cong 0.98$ as shown in Fig. 4. The results confirm that the damage process in the pillar is in metastable conditions according to a quasi-linear progression over time.

Statistical Distribution of AE Events: *b*-Value Analysis

Since the studies of Mogi and Scholz [25, 26] on AE, we know that the Gutenberg-Richter empirical law can be observed at the laboratory sample scale. They showed that a significant overlap exists between the definition of AE and earthquake. This is further reinforced by the evidence that brittle fracture obeys similar statistics from tectonic earthquakes to the dislocation movement smaller than micron size [27].

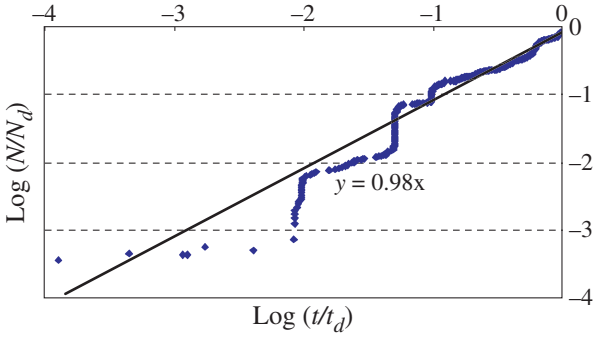

Figure 4: Evaluation of damage, β_t exponent for pillar 19

Moreover, in recent years, experiments employing acoustic emission have established remarkable results concerning the model of process zone and the quasi-static fault growth [28]. Such experiment-based knowledge is expected to be useful for studying the fundamental behaviour of natural earthquakes because it is widely accepted that fault systems are scale-invariant [29, 30] and there exist universal similarities between faulting behaviours, from small-scale microcracking to large-scale seismic faulting. For example, AE events caused by microcracking activity [25, 28–31] and stick-slip along a crack plane [32, 33] are similar to those generated by natural earthquakes.

AE frequency–magnitude statistics

By analogy with seismic phenomena, in the AE technique the magnitude may be defined as follows [34–37]:

$$m = \log_{10} A_{\max} + f(r), \quad (2)$$

where $A_{\max}$ is the amplitude of the signal expressed in μV and $f(r)$ is a correction coefficient whereby the signal amplitude is taken to be a decreasing function of the distance r between the source and the AE sensor. In seismology, the Gutenberg-Richter empirical law [38]:

$$\log_{10} N(\geq m) = a - bm \quad \text{or} \quad N(\geq m) = 10^{a-bm}, \quad (3)$$

expresses the relationship between magnitude and total number of earthquakes in any given region and time period, and is one of the most widely used statistical relations to describe the scaling properties of seismicity. In Equation (3), N is the cumulative number of earthquakes with magnitude $\geq m$ in a given area and within a specific time range, while a and b are positive constants varying from a region to another and from a time interval to another. Equation (3) has been used successfully in the AE field to study the scaling laws of AE wave amplitude distribution. This approach evidences the similarity between structural damage phenomena and seismic activities in a given region of the earth, extending the applicability of the Gutenberg-Richter law to structural engineering. According to Equation (3), the b-value changes systematically at different times

doi: 10.1111/j.1475-1305.2008.00602.x

in the course of the damage process and therefore can be used to estimate damage evolution modalities [34, 36].

Damage size-scaling

Scale effects on the size of the cracks identified by the AE technique entail, by analogy with earthquakes [38], the validity of the following relationship:

$$N(\geq L) = cL^{-2b}, \tag{4}$$

where N is the cumulative number of AE events generated by cracks having a characteristic size $\geq L$, c is the total number of AE events and $D = 2b$ is the noninteger (or fractal) exponent of the distribution. This interpretation rests on the assumption of a dislocation model for the seismic source and requires that $2 \leq D \leq 3$, i.e. the cracks are distributed in a fractal domain comprised between a surface and the volume of the analysed region [39].

The cumulative distribution (4) is substantially identical to the one proposed by Carpinteri [40, 41], according to which the number of cracks with size $\geq L$ present in a body is given by:

$$N^*(\geq L) = N_{\text{tot}}L^{-\gamma}, \tag{5}$$

In Equation (5), γ is an exponent reflecting the disorder, i.e. crack size scatter and N_{tot} is the total number of cracks present in a body. By equating distributions (4) and (5), we find that $2b = \gamma$. When the final propagation occurs, defects concentrate along preferential paths, in a narrow band around the final fracture surface. In this case, as shown by Carpinteri *et al.* [36, 37], the self-similarity condition entails $\gamma = 2.0$. This exponent corresponds to value $b = 1.0$, which is experimentally approached in structural members during the final crack propagation. In this connection, subdividing the loading process into consecutive stages, it is possible to explain the evolution of damage in terms of increasing microcrack density on preferential surfaces.

Laboratory Experimental Details

The stone used in the construction of the temple is calcareous in nature; archaeological studies have found the presence of various quarries of the Greek period in the area of Plemmirio, just south of Syracuse. During the recent restoration works, the technique of replacing stone blocks was employed for several damaged elements. The removed elements were replaced by other blocks of the same stone. In particular, a portion of one of the removed elements has been used to define, through laboratory tests, the mechanical properties of the material that after 2400 years still constitutes the bearing structure of the Cathedral. Some cylindrical specimens with diameter 30, 60 and 120 mm and slenderness $\lambda = 1$ were obtained from the stone block (Fig. 5). In particular, three specimens with a diameter of 30 mm ($S1_{a–c}$) and another three with a diameter of 60 mm ($S2_{a–c}$) were tested, while only two specimens with diameter of 120 mm ($S3_{a–b}$) were analysed. The specimens have been subjected to laboratory compressive tests at constant displacement rate of 4×10^{-4} mm s^{-1} and monitored by AE technique.

Results and discussion

The mechanical properties of the specimens were obtained by the stress–strain curves. In Fig. 6, the stress–strain curve together with the number of AE events cumulated during the test is reported for specimen $S2_a$. Similar behaviours are obtained for the other specimens. The experimental data obtained from the calcareous stone in compression indicate that this is a brittle material, as it exhibits a loss in load-carrying capacity when deformed beyond the peak load [42]. In particular, in Table 1 the experimental average values obtained from all compressive tests are shown. These values show that the peak stress decreases with increasing specimen size, while the dissipated energy, measured by the cumulative number of AE events at the peak load (N_{max}), increases. The interpretation of this size-dependent

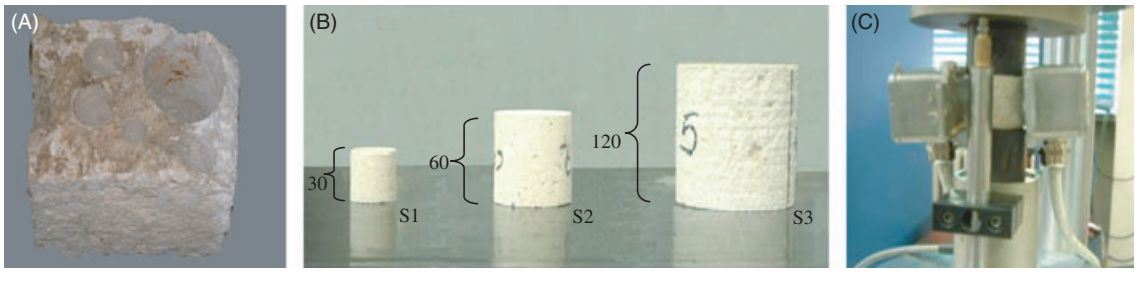

Figure 5: The stone block (A). Cylindrical specimens with diameters: 30, 60 and 120 mm and slenderness $\lambda = 1$ (B). AE sensors applied during the tests (C)

doi: 10.1111/j.1475-1305.2008.00602.x

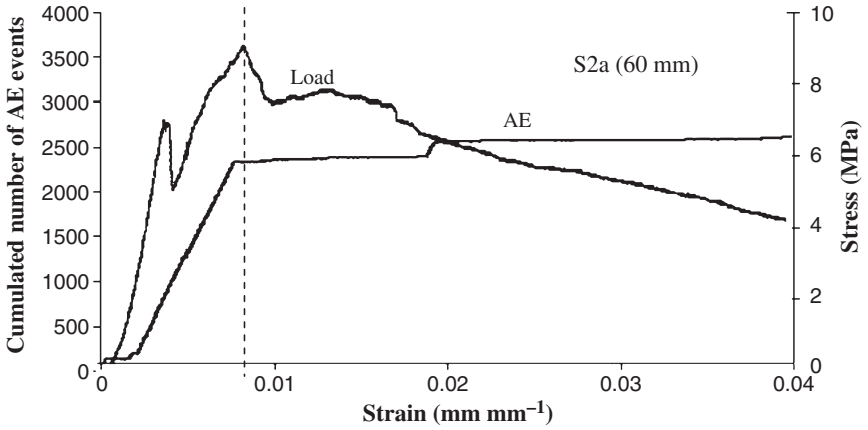

Figure 6: Stress versus strain curve and AE event cumulated number for the compression test on specimen $S2_a$

Table 1: Experimental average values obtained from compression tests

Specimens	Diameter (mm)	Volume (cm^3)	Peak load (kN)	Stress (MPa)	N_{max} at σ_u
$S1_{a–c}$	30	21.195	7.12	10.0	~500
$S2_{a–c}$	60	169.56	24.60	8.7	~2400
$S3_{a–b}$	120	1356.48	96.59	8.5	~10 200

behaviour through statistical and fractal approaches by the AE technique has been reported in other studies [23, 36, 37], in which the energy dissipation on a fractal domain for crushing tests on concrete was experimentally validated.

For all the tested specimens, the analysis of the *b*-value during the compression test was carried out. The '*b*-value' stands for the slope of the regression line in the 'log-linear' diagram of AE signal amplitude distribution [34–37]. The typical trends of the *b*-value during the tests conducted on specimens $S1_a$, $S2_a$ and $S3_a$ are shown in Fig. 7. The *b*-values, computed for sliding windows of 100 consecutive AE events, are reported together with the normalised load value (P/P_{max}) obtained during the tests. In other words, the *b*-values are determined in course of the tests by taking into account only current values and discarding the earlier ones. With this method, already adopted in other studies on the damage analysis in structural concrete elements [34], the testing time was subdivided into 5, 24 and 102 intervals (500, 2400 and 10 200, events) for specimens $S1_a$, $S2_a$ and $S3_a$, respectively.

In Fig. 7, the final *b*-value in the case of specimens $S1_a$ and $S3_a$ is <1.0, and approaches 1 for specimen $S2_a$ [36]. Figure 7 also shows that AE generated during the early stages of loading implies a high *b*-value >1.5 because of the closure of pre-existing micro-cracks in the rock [35], which causes several AE events with low amplitude.

In particular, the *b*-value obtained for the specimen $S2_a$ is greater than 2.5 immediately at the beginning of the test ($T/T_{max} \cong 0.1$ and $P/P_{max} \cong 0.05$); it reaches a value of 1.5 when $T/T_{max} \cong 0.8$ and $P/P_{max} \cong 0.5$ and finally tends to 1.0 at the end of the loading process. It can be noted that this anomalous behaviour is probably due to inhomogeneities contained in the calcareous stone [26] and also to the test

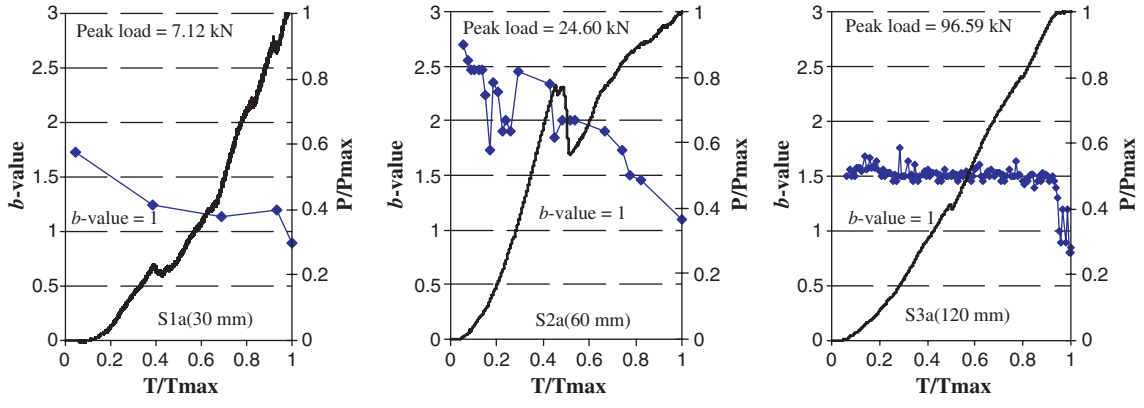

Figure 7: Normalised load value P/P_{max}, and trends of the *b*-value computed during the tests for specimens S1a, S2a and S3a

doi: 10.1111/j.1475-1305.2008.00602.x

type that is technically defined as 'compressive tests with rigid platens' (see Fig. 5C) [23]. In this kind of tests, no coupling material between the external surfaces of the specimens and the platens is used. When the specimen surfaces are not perfectly smooth and parallel, asymmetric stresses can take place in the inner part of the specimen during the loading phases. These asymmetric stresses are capable of producing ultrasonic noises because of the friction between the specimen surfaces and the rigid platens, altering AE signal detection. A similar behaviour is observed by Zhang *et al.* during asymmetric compressive loading tests on granite specimens [43]. In another paper by Jiang *et al.* [44], compressive tests on granite specimens are conducted by means of a triaxial servo-controlled loading apparatus. In this case too, *b*-values greater than 2.5 in the earlier phases of the tests are observed. The authors, in this case, impute the anomalies in the determination of *b*-values to the low value of the applied confinement pressure. Moreover, in a well-known paper of Lockner (Lockner *et al.* [28]) it is reported that during triaxial compressive tests on granite and sandstone 'the *b*-values for pre-nucleation events are indeed larger than for post-nucleation events, indicating a greater percentage of low amplitude events in the pre-nucleation phase'.

Equation (5) provides insight into the evolution of the crack size population during the development of cracking and damage, making it possible to interpret the experimentally observed variations in the *b*-value, expressed as $D/2$. Restricting the analysis to the interval $1.0 \leq b \leq 1.5$, which entails $2 \leq D \leq 3$, it can be seen that, in the subsequent phases of the loading process, when crack nucleation is the main mechanism, cracks are likely to be evenly spread throughout the volume of the specimens (*b*-value $\cong 1.5$ and $D \cong 3$). Furthermore, microcracks coalesce into larger and larger cracks and hence the *b*-value begins to decrease below 1.5. Immediately before the final collapse, the damaging process concentrates at the cracks near the final failure surface. It is possible to observe that a sudden drop in the *b*-value is found in the interval $0.8 \leq t/t_{max} \leq 1$ for all the specimens. At this point, microcrack coalescence is the main damage mechanism and strong localisation occurs. The number of cracks being proportional to the size of the element analysed, the *b*-value approaches 1.0 and the fractal dimension *D* of damage domain approaches 2. Moreover, the fact that during the final loading stages the *b*-value might drop below 1.0 (specimens $S1_a$ and $S3_a$) does not only mean an increase in damage, but also implies an increase in crack size [37]. Furthermore, the drop in the *b*-value below 1.0 can be explained by the fragmentation of the specimen and the effects of friction among them. These phenomena seem to reproduce, on a strongly reduced scale, the outline proposed by the theory of plate tectonics, where the Earth's surface is broken into large plates moving against each other [37].

Considering specimens of intermediate size (type S2), the AE distributions of signal amplitudes represented in Fig. 8A vary with the intensity reached by the load during the test. From the *b*-value computed using all the AE data collected at different levels of the load, we obtain the results shown in Fig. 8A. Similar results are obtained for all the other specimens (types S1 and S3). Then the *b*-value can be considered not only as an indicator of coalescence of fracture surfaces, but also as a good indicator of the level reached by the load during the test, independent of the specimen size. In Fig. 8B it can be observed that for all specimens, when the value of 80% of the ratio σ/σ_f is reached, the *b*-value invariably tends to 1.0.

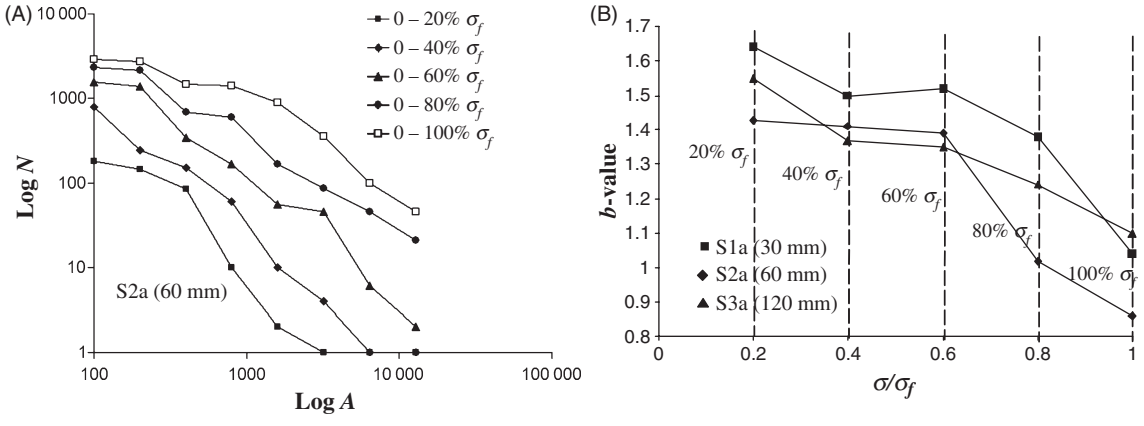

Figure 8: The AE distributions of signal amplitudes vary with the intensity reached by the load during the test for specimen $S2_a$ (A). In the same test, for the specimens $S1_a$, $S2_a$ and $S3_a$, when the value of 80% of the ratio σ/σ_f is exceeded, the *b*-value tends to 1.0 (B)

doi: 10.1111/j.1475-1305.2008.00602.x

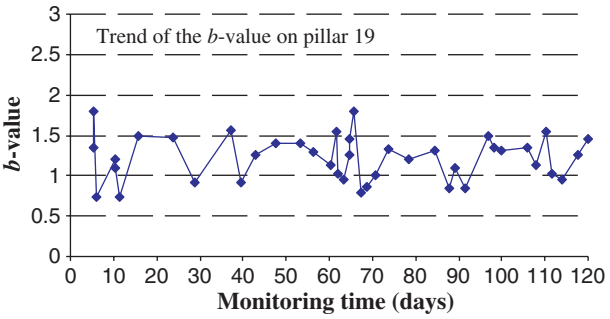

Figure 9: Trend of the *b*-value computed on pillar 19 during the monitoring time

Damage in the Monitored Pillar

The behaviour of the *b*-value computed from the data collected on pillar 19 during the monitoring is shown in Fig. 9. The oscillating pattern of the *b*-value confirms – as mentioned in the section *Detection and time dependence of damage* through the β_t exponent – that the damage process in the pillar is in meta-stable conditions and it could evolve into critical condition anytime. It can be noted, indeed, that the *b*-values are comprised between 1.5 and 1.0 during the monitoring period. Considering the relationship between the *b*-value and the stresses in the graph of Fig. 8B, and comparing it with the values assumed by the same parameter in the graph of Fig. 9, it is possible to recognise the *b*-value range in which the stress value exceeded the 80% of the ultimate strength. During the monitoring process conducted on pillar 19, a frequent seismic activity affected the area of Syracuse. Comparing Figs 3 and 8, it could be observed that each seismic event is followed by an increase in the level of damage implying a decrease in the *b*-value, which approaches 1.0. It is therefore reasonable that these loading conditions may have been the cause for compressive-bending stresses in the monitored pillar, with the achievement of stress levels close to the failure ones. In this way, the *b*-value can also be assumed to be a valid indicator of the stress level reached in the monitored structures.

Conclusions

The evolution of damage in a pillar made of calcareous stone blocks that is part of the vertical bearing structure of the Syracuse Cathedral was evaluated using the acoustic emission technique. With this technique it proved possible to acquire a great quantity of data during the monitoring process and subsequently perform a full analysis of the AE signals. In particular, a portion of one of the removed elements of the pillar has been used to define, through laboratory tests, the mechanical properties and the statistical distribution of AE data in the material that, after 2400 years, still constitutes the bearing structure of the Cathedral.

To assess the damage evolution of the pillar, two procedures are employed for the *in situ* and laboratory experiments. The first one concerns the *in situ* characterisation of the damage time dependence through the β_t exponent of Equation (1), the second one the estimation of the damage evolution through the *b*-value of Gutemberg-Richter's law. The data obtained during the *in situ* monitoring of the pillar show an exponent $\beta_t \cong 0.98$; this result confirms that the damage process in the pillar is metastable according to a quasi-linear progression over time.

In the second procedure, we consider the *b*-value as a fundamental parameter to evaluate the damage evolution and the stress levels reached in structural elements during the cracking process. Near the failure the *b*-value invariably tends to 1.0. This fact is experimentally demonstrated in this work both on the specimens extracted from the structure and on the structure itself. Recalling Equation (5) and the equality $D = 2b$, it is possible to explain the damage evolution in terms of crack distribution from the volume to preferential surfaces of the monitored element. In fact, when the final propagation occurs, defects concentrate along preferential paths, in a narrow band around the final fracture surface. The monitoring data obtained *in situ* also show that the *b*-value tends to 1.0 every time the stress in the pillar increases in concomitance of seismic activity, showing the achievement of stress levels close to the failure. Then through the study of the β_t parameter and the *b*-value we can appreciate both the damage time dependence and the stress level reached in the structure.

ACKNOWLEDGEMENTS

The financial support provided by the European Union (EU) Leonardo da Vinci Programme, ILTOF Project is gratefully acknowledged. Special thanks go to Prof. Luigia Binda of the Politecnico di Milano and to the Syracuse Superintendence for Cultural Heritage.

REFERENCES

1. Russo, S. (1991) La cattedrale di Siracusa. Archivio Storico Siracusano. III V, (in Italian).
2. Carpinteri, A. and Lacidogna, G. (2006) Damage monitoring of an historical masonry building by the Acoustic Emission technique. *Mater. Struct.* **39**, 161–167.
3. Carpinteri, A. and Lacidogna, G. (2006) Structural monitoring and integrity assessment of medieval towers. *J. Struct. Eng. (ASCE)* **132**, 1681–1690.

doi: 10.1111/j.1475-1305.2008.00602.x

4. Carpinteri, A. and Lacidogna, G. (2007) Damage evaluation of three masonry towers by acoustic emission. *Eng. Struct.* **29**, 1569–1579.
5. Binda, L. and Saisi, A. (1996) *Compatibility between Safety and Authenticity: The Experience of Noto Cathedral, Authenticity in the Restoration of Monuments, WTA*. Keynote Lecture, 2003. Wetenschappelijk–Technische Groep Voor Aanbevelingen, Leuven, 1–11.
6. Agnello, G. (1996) *Il Duomo di Siracusa e i suoi restauri*. Ediprint, Siracusa (in Italian).
7. Binda, L., Saisi, A. and Tiraboschi, C. (2000) Investigation procedures for the diagnosis of historic masonries. *Constr. Building Mater.* **4**, 199–233.
8. Binda, L., Lualdi, M., Saisi, A. and Zanzi, L. (2003) The complementary use of on site non destructive tests for the investigation of historic masonry structures, *Proc. 9th North Am. Masonry Conf.* (9NAMC), SC, USA, 978–989.
9. Binda, L., Cantini, L., Condoleo, P., Saisi, A. and Zanzi, L. (2006) Investigation on the pillars of the Syracuse Cathedral in Sicily. In: *3-Day International Conference on Structural Faults & Repair* (M. C. Forde, Ed.). Eng. Technics Press, Edinburgh, CD-ROM: 1–12.
10. Binda, L., Casolo, S., Petrini, V., Saisi, A., Sanjust, C. A. and Zanzi, L. (2004) Evaluation of the seismic vunerability of the Syracuse Cathedral. *Proc. Invest. Modelling Stud. Historical Heritage Int. Symp.*, Yildiz Technical University, Istanbul, Turkey, 683–690.
11. Carpinteri, A., Invernizzi, S., Lacidogna, G., Manuello, A. and Binda, L. (2008) Numerical simulation and monitoring of the Cathedral of Siracusa in Sicily. *6th Int. Conf. Struct. Anal. Historical Construction,* 2–4 July 2008, Bath, UK.
12. Carpinteri, A., Invernizzi, S., Lacidogna, G., Manuello, A. and Binda, L. (2008) Stability of the vertical bearing structures of the Syracuse Cathedral: experimental and numerical evaluation. *Mater. Struct.*, doi: 10.1617/s11527-008-9429-z.
13. Bieniawski, Z. T. (1967) Mechanism of brittle rock fracture. Part II. Experimental studies. *Int. J. Rock Mech. Mining Sci. Geomech. Abstr.* **4**, 407–423.
14. Brace, W. F., Paulding, B. W., Jr and Scholz, C. (1966) Dilatancy in the fracture of crystalline rocks. *J. Geophys. Res.* **71**, 3939–3953.
15. Scholz, C. H. (1968) Microfracturing and the inelastic deformation of rock in compression. *J. Geophys. Res.* **73**, 1417–1432.
16. Ohnaka, M. and Mogi, K. (1982) Frequency characteristics of acoustic emissions in rocks under uniaxial compression and its relation to the fracturing process to failure. *J. Geophys. Res.* **87**, 3873–3884.
17. Khair, A. W. (1984) Acoustic emission pattern: an indicator of mode of failure in geologic materials as affected by their natural imperfections. In: Proceedings of the 3rd Conference on Acoustic Emission/ Microseismic Activity in Geologic Structures and Materials, 1981, University Park, PA (H. R. Hardy Jr and F. W. Leighton, Eds). Trans Tech Publications, Clausthal: 45–66.
18. Eberhardt, E., Stead, D., Stimpson, B. and Read, R. S. (1998) Identifying crack initiation and propagation thresholds in brittle rock. *J. Can. Geotech.* **35**, 222–233.
19. Anzani, A., Binda, L., Carpinteri, A., Lacidogna, G. and Manuello, A. (2008) Evaluation of the repair on multiple leaf stone masonry by acoustic emission. *Mater. Struct. (RILEM)* **41**, 1169–1189.
20. Landis, E. N. and Shah, S. P. (1995) Frequency-dependent stress wave attenuation in cement-based materials. *J. Eng. Mech.* **121**, 737–743.
21. Brindley, B. J., Holt, J. and Palmer, I. G. (1973) Acoustic emission-3: the use of ring-down counting. *Non-Destructive Testing* **6**, 299–306.
22. Pollock, A. A. (1973) Acoustic emission-2: acoustic emission amplitudes. *Non-Destructive Testing* **6**, 264–269.
23. Carpinteri, A., Lacidogna, G. and Pugno, N. (2007) Structural damage diagnosis and life-time assessment by acoustic emission monitoring. *Eng. Fract. Mech.* **74**, 273–289.
24. Carpinteri, A., Lacidogna, G. and Paggi, M. (2006) Acoustic emission monitoring and numerical modelling of FRP delamination in RC beams with non-rectangular cross-section. *Mater. Struct.* **40**, 553–566.
25. Mogi, K. (1962) Magnitude frequency relations for elastic shocks accompanying fractures of various materials and some related problems in earthquakes. *Bull. Earthquake Res. Inst. Univ. Tokyo* **40**, 831–853.
26. Scholz, C. H. (1968) The frequency-magnitude relation of microfracturing in rock and its relation to earthquakes. *Bull. Seismol. Soc. Am.* **58**, 399–415.
27. Miguel, M. C., Vespignani, A., Zapperi, S., Weiss, J. and Grasso, J. R. (2001) Intermittent dislocation flow in viscoplastic deformation. *Nature* **410**, 667–670.
28. Lockner, D. A., Byerlee, J. D., Kuksenko, V., Ponomarev, A. and Sidorin, A. (1991) Quasi static fault growth and shear fracture energy in granite. *Nature* **350**, 39–42.
29. Hirata, T. (1989) Fractal dimension of fault system in Japan: fracture structure in rock fracture geometry at various scales. *Pure Appl. Geophys.* **131**, 157–170.
30. Bonnet, E., Bour, O., Odling, N. E., Davy, P., Main, I., Cowie, P. and Berkowitz, B. (2001) Scaling of fracture systems in geological media. *Rev. Geophys.* **39**, 347–383.
31. Lei, X. (2003) How do asperities fracture? An experimental study of unbroken asperities. *Earth Planet. Sci. Lett.* **213**, 347–359.
32. Kato, N., Yamamoto, K. and Hirasawa, T. (1994) Microfracture processes i the break down zone during dynamic shear rupture inferred from laboratory observation of near-fault high-frequency strong motion. *Pure Appl. Geophys.* **142**, 713–734.
33. Lei, X. L., Nishizawa, O., Kusunose, K., Cho, A. and Satoh, T. (2000) On the compressive failure of shale samples containing quartz-healed joints using rapid AE monitoring: the role of asperities. *Tectonophysics* **328**, 329–340.
34. Colombo, S., Main, I. G. and Forde, M. C. (2003) Assessing damage of reinforced concrete beam using ''*b*-value'' analysis of acoustic emission signals. *J. Mat. Civil Eng. (ASCE)* **15**, 280–286.

doi: 10.1111/j.1475-1305.2008.00602.x

35. Rao, M. V. M. S. and Lakschmi, P. K. J. (2005) Analysis of *b*-value and improved *b*-value of acoustic emissions accompanying rock fracture. *Curr. Sci. – Bangalore* **89**, 1577–1582.
36. Carpinteri, A., Lacidogna, G., Niccolini, G. and Puzzi, S. (2008) Critical defect size distributions in concrete structures detected by the acoustic emission technique. *Meccanica* **43**, 349–363.
37. Carpinteri, A., Lacidogna, G., Niccolini, G. and Puzzi, S. (2008) Morphological fractal dimension versus power-law exponent in the scaling of damaged media. *Int. J. Damage Mech.* (in press).
38. Richter, C. F. (1958) *Elementary Seismology*. W.H. Freeman, San Francisco, CA; and London.
39. Rundle, J. B., Turcotte, D. L., Shcherbakov, R., Klein, W. and Sammis, C. (2003) Statistical physics approach to understanding the multiscale dynamics of earthquake fault systems. *Rev. Geophys.* **41**, 1–30.
40. Carpinteri, A. (1994) Scaling laws and renormalization groups for strength and toughness of disordered materials. *Int. J. Solids Struct.* **31**, 291–302.
41. Carpinteri, A. (1986) *Mechanical Damage and Crack Growth in Concrete: Plastic Collapse to Brittle Fracture*. Martinus Nijhoff Publishers, Dordrecht.
42. Hudson, J. H., Crouch, L. S. and Faihurst, C. (1972) Soft, stiff and servo controlled testing machines: a review with reference to rock failure. *Engineering Geolgy* **6**, 155–189.
43. Zhang, A., Wagner, F. C., Stanchits, S., Dresesn, G., Andrsen, R. and Haidekker, M. A. (1998) Source analysis of acousic emission in aue granite cores under symmetric and asymmetric compressive load. *Geophys. J. Int.* **135**, 1113–1130.
44. Jiang, H., Zhang, L. and Zhou, Y. (2000) Granite deformation and behaviour of acoustic emission sequence under the temperature and pressure condition at different crust depths. *Acta Seismol. Sin.* **13**, 424–433.

doi: 10.1111/j.1475-1305.2008.00602.x